J. Nanoanalysis., 6(1): 21-32, Winter 2019

ORIGINAL RESEARCH PAPER

Structural, Magnetic and Catalytic Properties of Non-Stoichiometric Lanthanum Ferrite Nano-Perovskites in Carbon Monoxide Oxidation

Zahra Ramezani [1], Azim Malekzadeh [1,*], Mahnaz Ghiasi [2], Ahmad Gholizadeh [3], Elham Ghiasi [1]

[1] School of Chemistry, Damghan University, Damghan, Iran

[2] Inorganic Chemistry and Catalysis, Debye Institute for Nanomaterials Science, Utrecht University, Universiteitsweg 99, Utrecht 3584 CG, The Netherlands

[3] School of Physics, Damghan University, Damghan, Iran

Received: 2018-04-25 Accepted: 2018-12-13 Published: 2019-02-01

ABSTRACT

Perovskite-type oxides of $LaFe_{(1+x)}O_{(3+\delta)}$ (x = 0.0, 0.2, 0.5 and 0.7) were synthesized by citrate sol–gel method to ensure the formation of nanosized perovskites. The physicochemical properties of these $LaFe_{(1+x)}O_{(3+\delta)}$ materials were characterized by thermal gravimetric/differential analyses, Fourier transform infrared spectroscopy, X-ray powder diffraction, scanning electron and transmission electron microscopies, ultraviolet-visible spectroscopy, Brunauer Emmett Teller nitrogen absorption, electrical conductivity measurements and magnetic studies. Catalytic performances of the prepared materials were evaluated for the carbon monoxide oxidation. Trace of $FeCO_3$ and Fe_2O_3 phases were detected over the perovskites of $LaFe_{(1+x)}O_{(3+\delta)}$ with excess iron (x > 0) using the XRD and FT-IR studies. The SEM results demonstrate the formation of non-spongy particles. The magnetic measurements show a charge ordering transition at ~230 K for $LaFe_{1.2}O_{(3+\delta)}$ perovskite. The weak long range charge ordering of Fe^{2+}/Fe^{3+} destroys over an increase in the content of the phases other than $LaFeO_3$ perovskite. The best σ_{ox}/σ_{Red} and the lowest E_c is accounted for the more suitable path for catching and giving of the gas phase oxygen over $LaFe_{1.2}O_{(3+\delta)}$ nanoperovskite; meaning most favorable redox properties. The light off temperature of the CO oxidation in terms of reducibility studies is decreased about 70°C over crystalline $LaFe_{1.2}O_{(3+\delta)}$ catalyst.

Keywords: *Catalytic CO Oxidation; Electrical Conductivity; $LaFeO_3$; Magnetic Measurements; Nanoperovskite; Nonstoichiometry*

How to cite this article

Ramezani Z, Malekzadeh A, Ghiasi M, Gholizadeh A, Ghiasi E. Structural, Magnetic and Catalytic Properties of Non-Stoichiometric Lanthanum Ferrite Nano-Perovskites in Carbon Monoxide Oxidation. J. Nanoanalysis., 2019; 6(1): 21-32.
DOI: 10.22034/jna.2019.664398

INTRODUCTION

The catalytic oxidation of CO has wide applications in indoor air cleaning [1], CO gas sensors [2], automotive exhaust treatment and etc. [3]. Supported precious metal catalysts have been investigated for various chemical reactions [4,5]. Perovskites are known as promising alternatives to supported noble metals for many applications because of their low cost, thermal stability, great versatility and excellent redox properties [6-8]. The research efforts concentrated on the perovskite family, ABO_3, where A = rare-earth and B = transition metal, are important in advanced technologies such as fuel cells, catalysis, electrode materials, and sensors [4,7-8].

The catalytic properties of perovskites were systematically studied since 1977 and they have been widely used for total oxidation reactions [7-8]. The $LaMO_3$ perovskites (M: transition metal) are particularly active in oxidative catalysis if M can fluctuate between two stable oxidation states, such as Fe^{2+} and Fe^{3+} in this case [9]. An orthorhombic

* Corresponding Author Email: *malekzadeh@du.ac.ir*

$LaFeO_3$ perovskite was obtained by solution combustion technique from metal nitrates in fuel-rich conditions [10-11]. Any phase modification was not observed in the annealed sample at 400°C for 3 h. Particle size of 42 nm and specific surface area of about 4 m^2/g were reported for a low temperature calcined sample. The non-stoichiometric perovskites, which can easily release oxygen, are more active than that of the stoichiometric one [9]. Synthesis of metal oxide nanoparticles in the presence of organic additives is a simple method in process and low in cost, which saves time and reduces energy consumption. This method enables a good chemical homogeneity and a narrow particle size distribution [10-11]. Organic compounds that form complex with metal cations facilitate homogeneous mixing of the cations and impede the preferential precipitation of ionic species in solution [12].

Polycrystalline $La_{(1-x)}FeO_{(3-1.5x)}$ perovskites with x = 0.0, 0.1, 0.2 and 0.3 were prepared via the low-temperature thermal decomposition of La and Fe nitrates and final calcination at 600°C for 24 h [9]. The best catalytic activity for methane combustion was reported for $La_{0.9}FeO_{2.85}$ sample. In this study, a representative type of perovskite, namely $LaFeO_3$, has been chosen. The effect of excess Fe in the $LaFe_{(1+x)}O_{(3+\delta)}$ perovskite oxides on catalytic activity for oxidation of carbon monoxide was investigated. The samples were synthesized in the presence of citric acid, a method known as citrate sol-gel method, and were structurally characterized. An explanation of oxidation properties was provided in term of electronic, structural and magnetic features.

MATERIALS AND METHODS

All reagents were of analytical grade and used without further purification. The samples of $LaFe_{(1+x)}O_{(3+\delta)}$ with x = 0.0, 0.2, 0.5 and 0.7 were prepared by the citrate method according to Table 1 [13]. Solutions containing appropriate concentrations of metal nitrates and citric acid, equal to the total number of moles of nitrate ions, were evaporated at 60°C overnight. The homogeneous gel-like substances were dried at 80°C overnight. The resulting spongy and friable materials were completely powdered and kept at 160°C overnight. The final powdered materials were subsequently calcined at 600, 800 and 900°C for 5 h.

Thermogravimetric (TG) and differential thermal analysis (DTA) of the precursor compounds, dried at 160°C, were carried out using thermal gravimetric/differential instrument (BÄHR-Thermoanalyse GmbH Model STA 503). The samples were heated continually with a heating rate of 10°C/min from room temperature to 800°C in a static air atmosphere. The FT-IR spectra of samples were recorded on a Perkin-Elmer FT-IR spectrometer in the wavenumber range of 400-2000 cm^{-1}. The phase quality of the freshly calcined samples was examined by powder X-ray diffraction analysis in the angle range of 2θ = 20-80° using a Bruker AXS diffractometer D8 ADVANCE with Cu-Kα radiation filtered by a nickel monochromator and operated at 40 kV and 30 mA. The XRD data were analyzed using a commercial Xpert package and Fullprof program. The information on microstrain (ε_s) and crystallite size (D) of the powders have been obtained from the full-width at half-maximum (FWHM) of the diffraction peaks (β) via Williamson-Hall relation [13]. The crystallite size of the powders was also calculated by the Scherrer's equation. The morphology and particle size of the samples

Table 1. Experimental conditions for the preparation of $LaFe_{(1+x)}O_{(3+\delta)}$ samples. Here x = 0.0, 0.2, 0.5 and 0.7. Mole number of $La(NO_3)_3 \cdot 6H_2O$ was kept to be 0.008 in all preparations.

Sample	Sample number	Calcination temperature (°C)	Mole of $Fe(NO_3)_3 \cdot 9H_2O$	Mole of Citric acid
	1	600		
$LaFeO_3$	5	800	0.0080	0.0480
	9	900		
	2	600		
$LaFe_{1.2}O_{3+\delta}$	6	800	0.0096	0.0528
	10	900		
	3	600		
$LaFe_{1.5}O_{3+\delta}$	7	800	0.0120	0.0600
	11	900		
	4	600		
$LaFe_{1.7}O_{3+\delta}$	8	800	0.0136	0.0648
	12	900		

were studied using SEM (Philips XL30) and TEM (LEO Model 912AB) analyses, respectively. The electric conductivity of the samples was measured according to literature [14]. Magnetic studies involving temperature dependent magnetization in the temperature range of 10-400 K and hysteresis loops at room temperature and 10 K were carried out using a SQUID magnetometer.

Catalytic CO oxidation tests over $LaFe_{(1+x)}O_{(3+\delta)}$ catalysts were studied using a quartz tube as a continues flow reactor, filled with 200 mg of 60-100 mesh sized catalyst supported on ceramic wool. The reactor was placed at the middle of an electric furnace. The temperature of the furnace was controlled using a PID Atbin controller. In a typical experiment, a gaseous mixture of 6%CO in Ar and air, with a stoichiometric ratio with respect to oxygen, was passed through the catalyst bed with a total gas mixture flow rate of 40 mL (STP)/min; i.e. a GHSV = 12000 $\left(\frac{mL}{g_{Cat}\cdot h}\right)$ and a contact time of 0.3$\left(\frac{g_{Cat}\cdot s}{mL}\right)$. Catalytic tests were carried out using temperature rising at randomly intervals of time from 50°C to temperature of complete oxidation of carbon monoxide. The product stream was analyzed using a gas chromatograph (GC) equipped with a FI detector and a methanizer in an off line format. The sampling was carried out under steady state condition at a constant temperature. The reaction is completed in a narrow range of temperature and the temperature rising is a more important parameter than time intervals. Thus, the temperature rising was carried out too slow, 2° in each step of temperature rising, near the temperature at which the reaction is almost completed. Any carbon dioxide was not detected using an empty reactor equipped with the ceramic wool; a blank run.

RESULTS AND DISCUSSION

Fig. 1 shows the thermal gravimetric analysis curves of the dried samples at 160°C, coupled with the differential thermal analysis. The sequential weight loss are observed to be exothermic. The formation of metal carboxylates is known as a result of interaction between metal cations and citric acid [15]. The dried samples at low temperature can

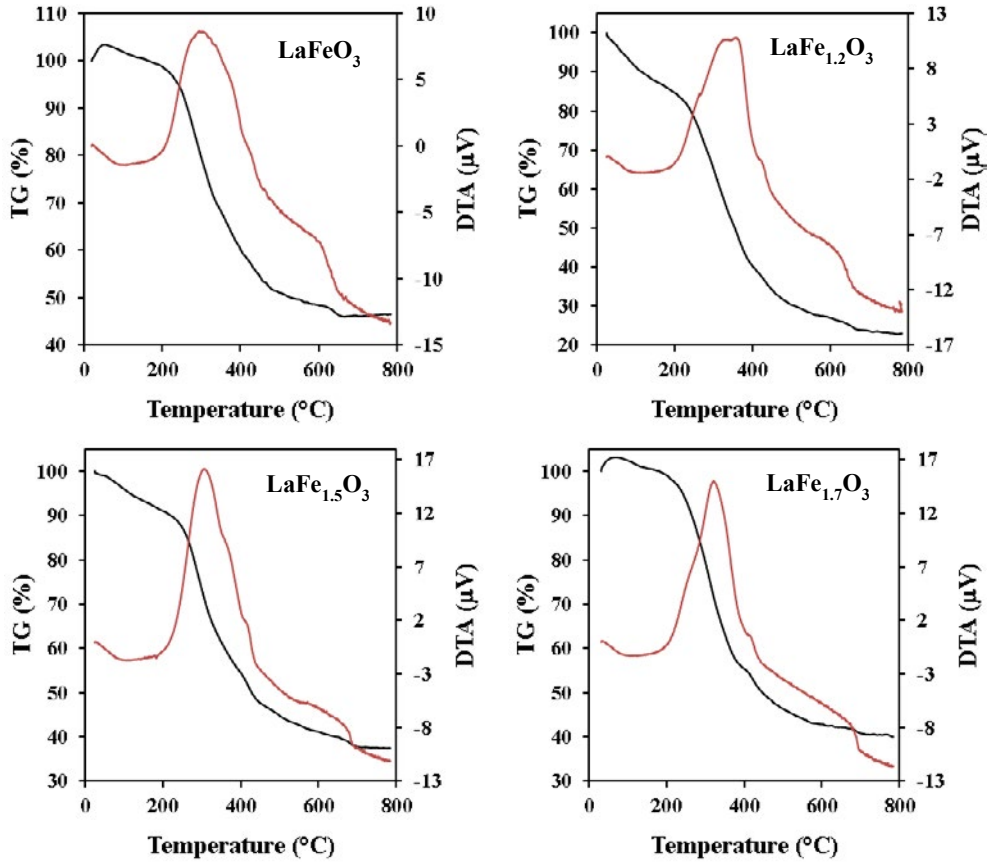

Fig. 1. TG/DTA of precursor materials (samples after drying at 160°C).

be considered as metal nitrates and / or citrates. Considering a formula is almost impossible for the samples that dried at 160°C. Thus, the weight loss results cannot be compared with the calculated metal citrate or / and nitrate. The main weight loss, however, happens around 400°C. The slope of the weight loss decreases sharply at ~600°C and the final product seems to form at temperatures greater than 750°C. Accordingly, the samples were first calcined at 600°C.

X-ray diffraction patterns of the samples after calcining at 600°C and 800°C (samples 1-8) are shown in Fig. 2. In agreement with the TG-DTA analysis, low crystallinity is observed for the samples that were calcined at 600°C (Fig. 2, samples 1-4); samples $LaFe_{1.5}O_3$ (# 3) and $LaFe_{1.7}O_3$ (# 4) are observed to be completely amorphous. The crystallinity, however, increases after calcining at 800°C (Fig. 2, samples 5-8). Some impurity of $La_2O_2CO_3$ is observed after calcination at 800°C. Rietveld analyzed X-ray diffraction patterns of the samples after calcining at 900°C are presented in Fig. 3. Any crystalline phase of $La_2O_2CO_3$ was

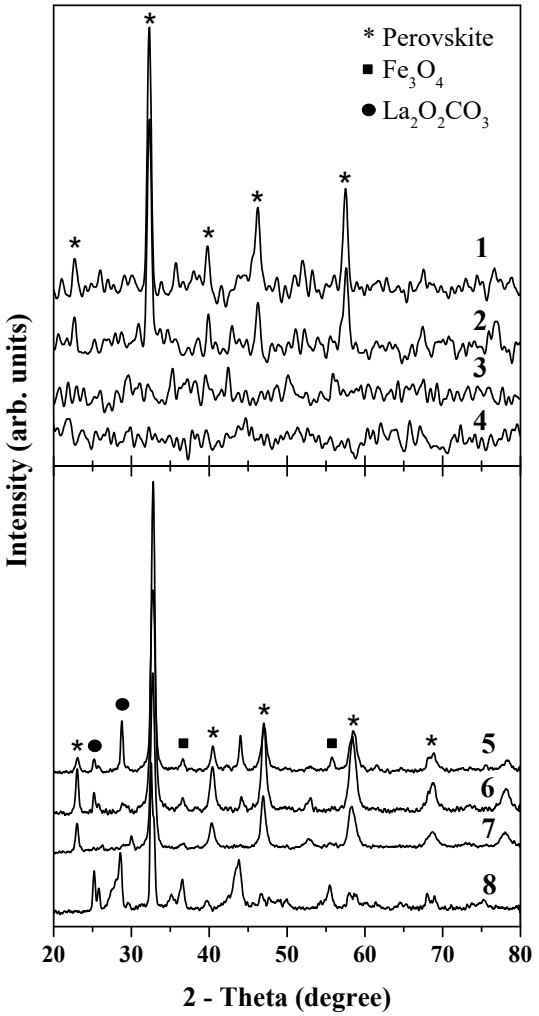

Fig. 2. X-ray diffraction patterns of samples 1-8 in Table 1.

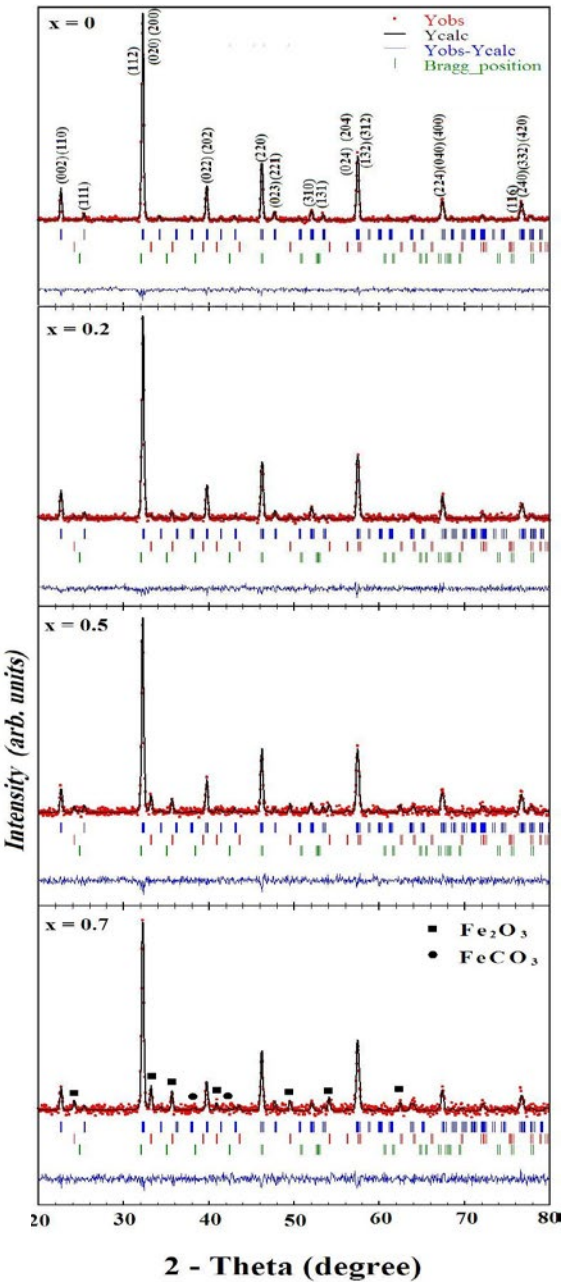

Fig. 3. Rietveld analysis of the X-ray diffraction patterns of samples 9-12 of Table 1. The circle sings represent the raw data. The solid line represents the calculated profile. Vertical bars indicate the position of Bragg peaks for the perovskite orthorhombic and Fe_2O_3 rhombohedral structures. The lowest curve is the difference between the observed and the calculated patterns. The indices (h k l) of the orthorhombic phase are written above the peaks.

not detected after calcination at 900°C. The small amount of $FeCO_3$, however, is observed after calcining at 900°C. Fig. 3 shows that the diffraction patterns of the main phase for the stoichiometric and non-stoichiometric samples using both the Xpert package and Fullproof program can be quite well indexed to an orthorhombic perovskite structure; space group of Pbnm with the unit cell parameters of a = 5.55 Å, b = 5.56 Å and c = 7.86 Å. The diffraction data are in good agreement with JCPD card of $LaFeO_3$; JCPDS No.37-1493. Crystalline phase of rhombohedral Fe_2O_3 (space group of R-3c, unit cell parameters of a = 5.426 Å and α = 55.27°) is detected upon an increase in the mole number of the non-stoichiometric iron cations.

The crystallite size and microstrain of the samples that calcined at 900°C (# 9-12) are presented in Table 2. The negative values of the strain, ε, are related to a decrease in the length / width ratio of the samples and show that the peak broadening is mainly due to the lattice shrinkage [16]. The strain is reached to a maximum in sample 10 and is not affected upon further increase in the nonstochemitric iron content. It is related to the presence of the Fe_2O_3 phase. The excess iron more than 0.2 mole number has not a considerable effect on the lattice shrinkage.

Further investigation on the composition of prepared samples was carried out using vibrational spectroscopy (Fig. 4). The broadband at 520-680 cm^{-1} is assigned to Fe-O asymmetrical stretching vibration [12-13]. A band at ~400 cm^{-1} is related to Fe-O-Fe deformation vibration. The bands are completely broadened for the samples that calcined at 600°C (# 1-4). The IR characteristics at 520-680 cm^{-1} are assigned to the stretching mode of the FeO_6 octahedron in the $LaFeO_3$ or Fe_2O_3 structure. A sharper band in the FT-IR spectrum of perovskites was related to a more symmetrical

Table 2. Crystallite size[a] (nm) and microstrain (ε) of the perovskite phase of $LaFe_{(1+x)}O_{(3+\delta)}$ samples

	Scherrer Method	Williamson-Hall Method	
Sample no.	D (nm)	D (nm)	ε (no unit) ×100
9	47	32	-0.049
10	45	25	-0.140
11	42	25	-0.142
12	38	25	-0.143

[a]The calculated crystallite size by the Scherrer equation is an average value. The calculations were performed using perovskite peaks in Fig. 3.

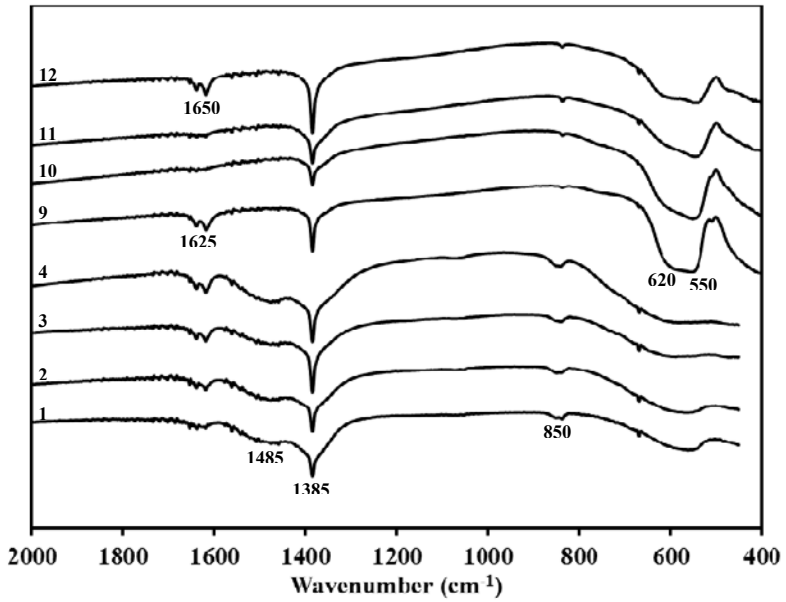

Fig. 4. FT-IR spectra of samples 1-4 and 9-12 of Table 1.

structure while widening of this band was reported to be an indication of a structure with lower symmetry [17]. The bands around 1485, 1385 and 850 cm^{-1} correspond to the principal vibrations of carbonate group, indicating the existence of carbonate species on the $LaFeO_3$ surface [12-13]. The bands at ~1625 and 1650 cm^{-1} can be related to the surface-adsorbed oxygen species [18].

Images of the electron microscopies and the histogram of the particle size distribution of the samples $LaFeO_3$ (No. 9 in Table1) and $LaFe_{1.2}O_3$ (No. 10 in Table1) after calcining at 900°C are shown in Figs. 5-1 and 5-2. Scanning electron microscopic results show that the powders are almost spherical and non-spongy with a uniform grain size distribution and homogeneous microstructure. TEM was employed to obtain direct information regarding to the size and structure of samples 9 and 10. It shows mono-dispersed particles with an average size of about 65 nm (sample 9) and 55 nm (sample 10). A disagreement is observed with the average size obtained from the peak broadening in

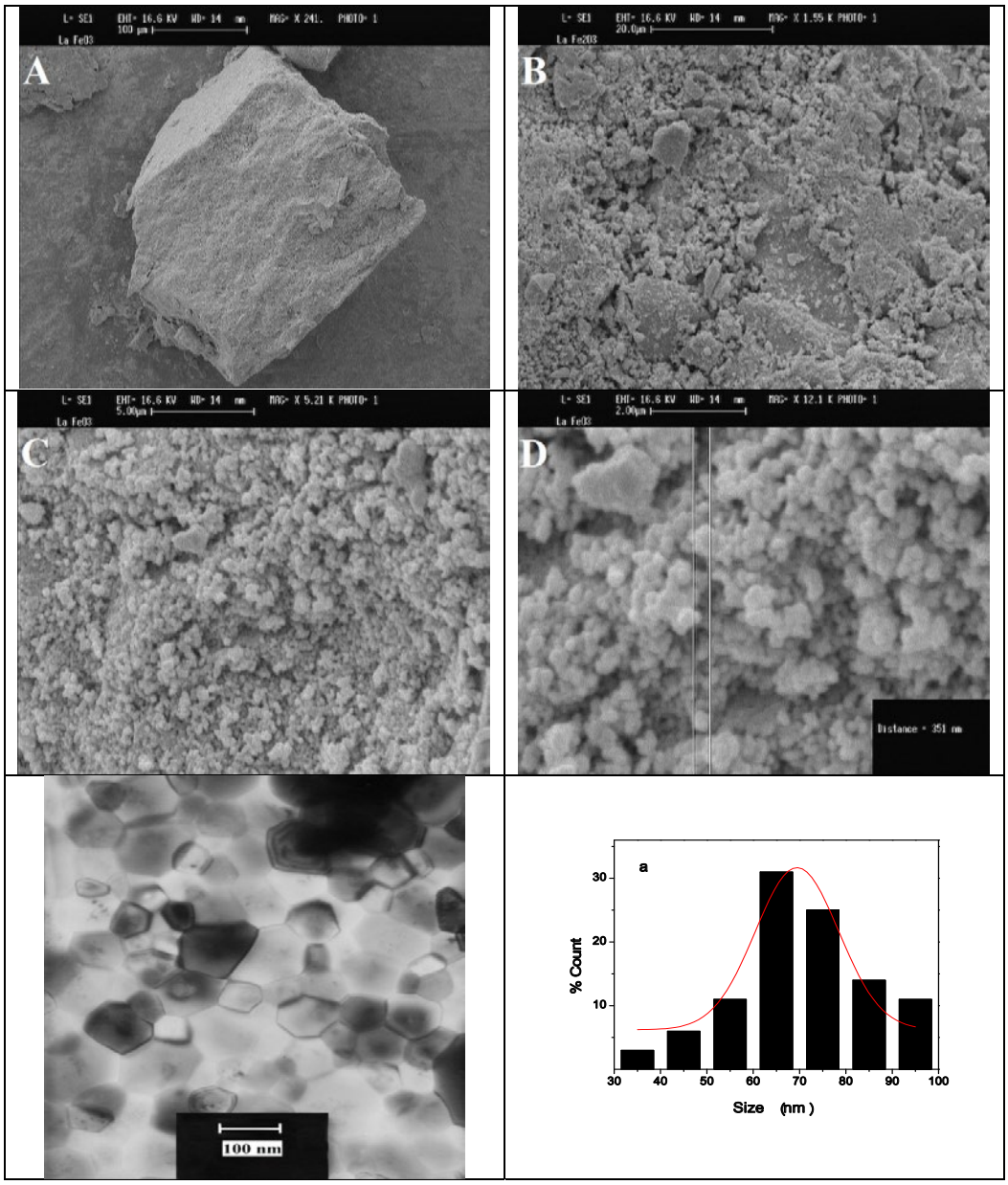

Fig. 5-1. SEM results, TEM micrograph and size distribution histogram of $LaFeO_3$ (# 9 in Table 1) sample.

X-ray study. The difference comes from the fact that TEM and XRD measure particles and crystallites size, respectively. One particle can be constituted by several crystalline domains (crystallites). TEM micrographs show the spherical, spheroidal and polygon morphologies for the prepared nanoparticles.

Fig. 6 shows the hysteresis loops of the $LaFe_{(1+x)}O_{(3+\delta)}$ nanocrystals (samples 9-12) at room temperature and 10 K, respectively. The super paramagnetic behavior of the stoichiometric lanthanum ferrite, which is observed at room temperature, changes to a paramagnetic one upon increasing of the x in $LaFe_{(1+x)}O_{(3+\delta)}$ samples. The form of the low temperature hysteresis loop is a characteristic of a weak ferromagnetism (WFM) for $LaFeO_3$ and $LaFe_{1.2}O_{(3+\delta)}$ samples. Ferromagnetic behavior, however, turns to an antiferromagnetic one upon an increase in the mole of the Fe cation. It is related to the presence of Fe_2O_3 species. The non-saturation of the magnetization is also a characteristic of antiferromagnetic (AFM) ordering

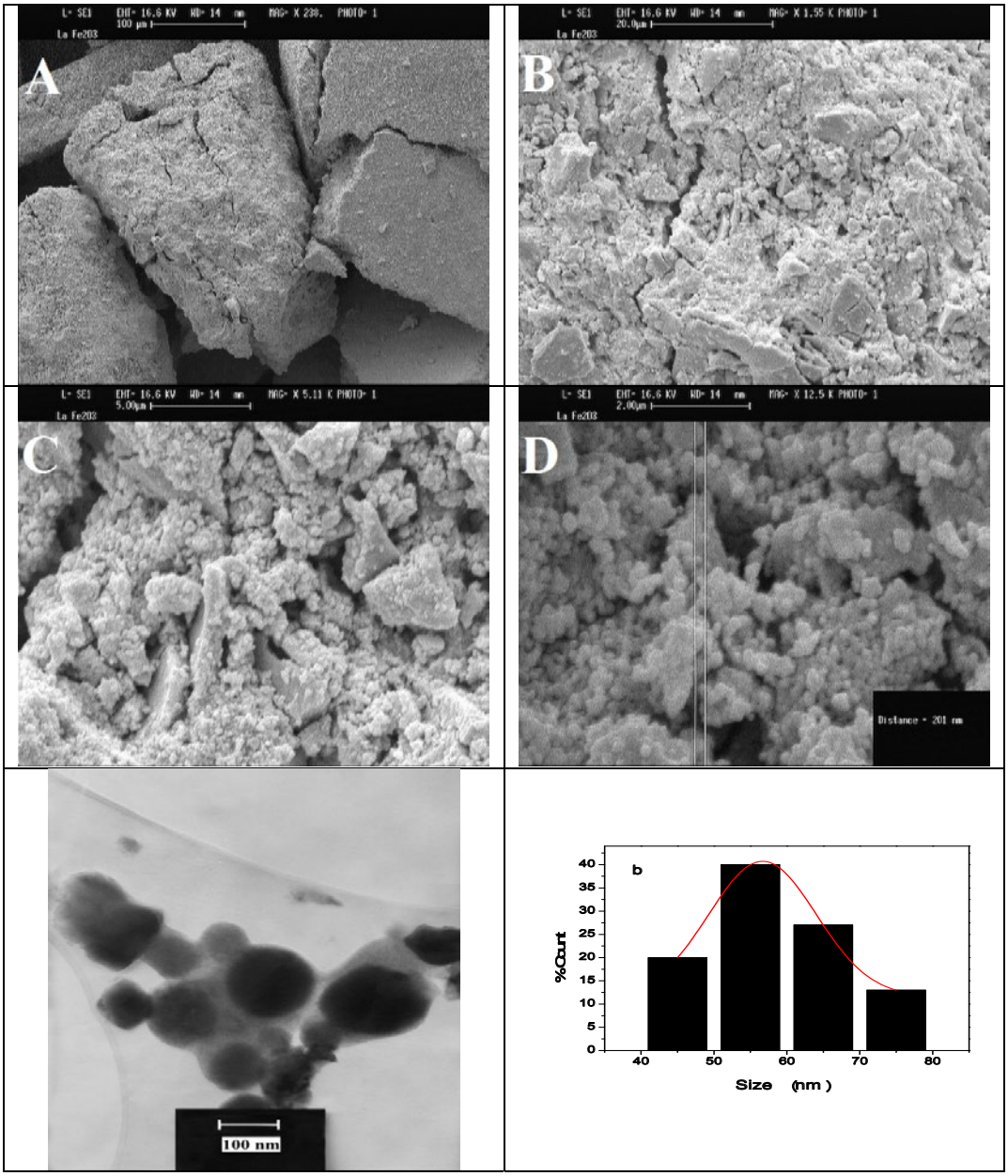

Fig. 5-2. SEM results, TEM micrograph and size distribution histogram of $LaFe_{1.2}O_3$ sample (# 10 in Table 1).

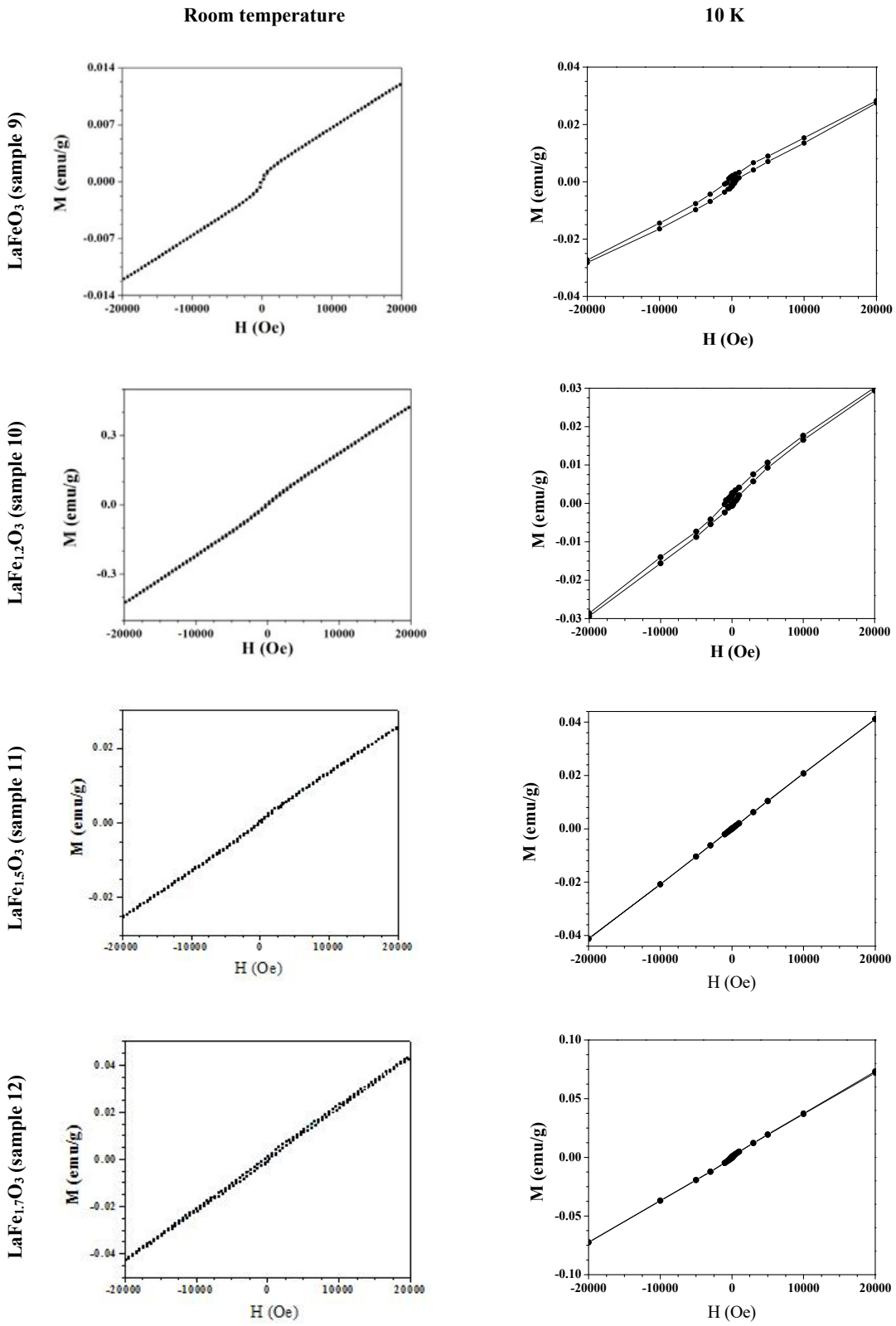

Fig. 6. The curves of magnetization versus applied filed (M-H) at room temperature (▪▪▪▪▪▪▪▪) and 10 K (——) for samples that calcined at 900°C (# 9-12 of Table 1).

of the spins in these samples [19].

Fig. 7 shows the temperature dependence of magnetization in a magnetic field of 1000 Oe between 10 to 400 K for $LaFe_{(1+x)}O_{(3+\delta)}$ samples that calcined at 900°C (samples 9-12). A decrease of the temperature leads to an increase in the magnetization of $LaFeO_3$ nanocrystals. A charged ordering transition is only observed for $LaFe_{1.2}O_{(3+\delta)}$ perovskite at ~230 K. The mixed valence character of the B-site (Fe^{2+}/Fe^{3+}) forms a weak long range charge ordering of Fe^{2+} and Fe^{3+} in non-stoichiometric $LaFe_{(1+x)}O_{(3+\delta)}$ samples [20,21]. An increase in the content of the phases other than perovskite destroys the long range charge ordering in $LaFe_{(1+x)}O_{(3+\delta)}$ samples. It is completely observed the samples with $x > 0.2$.

The oxidation state of the iron cations in fresh $LaFe_{(1+x)}O_{(3+\delta)}$ nano-powders were investigated by the reflectance electron absorption spectroscopy (Fig. 8). Broad absorption peaks of the $LaFe_{(1+x)}O_{(3+\delta)}$ nanocrystals at ~360, 460 and 550 nm indicate that the prepared catalysts can be categorized as photocatalytic materials [19]. Region 1 in the wavelength range of 300-400 nm assign to the

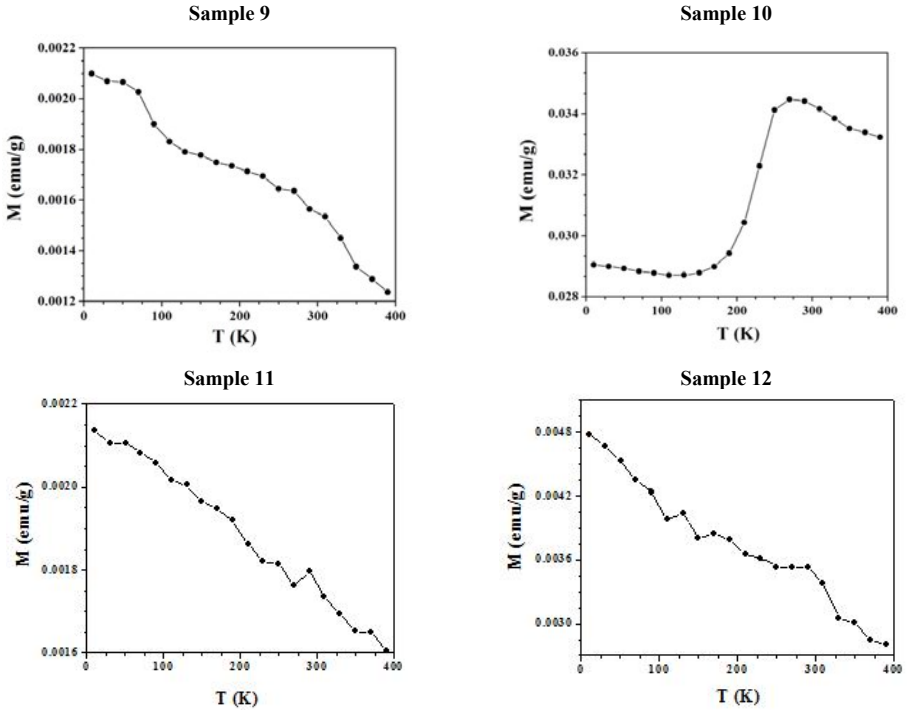

Fig. 7. Temperature dependence of magnetization in a magnetic field of 1 kOe for samples that calcilned at 900°C (# 9-12 of Table 1).

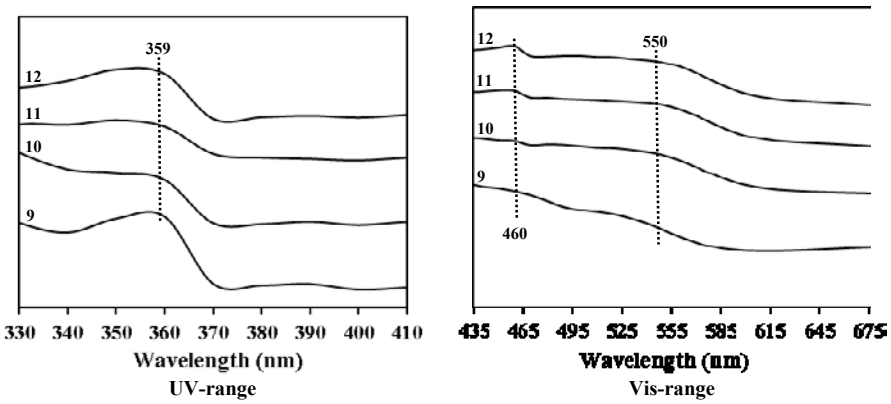

Fig. 8. UV-Vis spectra of samples 9-12 reported in Table 1 for the wavelenght of 330-410 nm (charge transfer) and 435-675 nm (d-d transitions).

ligand to metal charge transfer (LMCT) transitions and less contribution comes from the Fe^{3+} ligand field transitions $^6A_1 \rightarrow {}^4T_1(^4P)$, $^6A_1 \rightarrow {}^4E(^4D)$ and $^6A1 \rightarrow {}^4T_2(^4D)$, respectively [20,21]. Absorptions between 400-700 nm appoint to the pair excitation in the form of $^6A_1 + {}^6A_1 \rightarrow {}^4T_1(^4G) + {}^4T_1(^4G)$ process [22]. It is related to the overlap of the tail of charge-transfer band with the ligand field transitions of $^6A_1 \rightarrow {}^4E(^4G)$ and $^6A_1 \rightarrow {}^4A_1(^4G)$.

The catalytic activity of the prepared samples was studied for the oxidation of carbon monoxide. Table 3 shows the temperature of 10%, 50%, and 90% conversion to carbon dioxide. The temperature corresponding to 50% conversion is defined as the light off temperature of catalyst, known as an important parameter in catalytic reactions [9]. The lower the light off temperature, the more active the catalyst is. The XRD results show that the crystallinity, extent of the crystallization, depends on the calcination temperature. Amorphous feature is observed for $LaFe_{1.5}O_3$ (sample 3) and $LaFe_{1.7}O_3$ (sample 4) after calcining at 600°C. Instead, more crystalline samples are obtained upon calcination at higher temperature. Crystallization is accompanied by a better catalytic activity. Results of the XRD analysis and Table 3 show that the formation of a more crystalline perovskite phase is a necessity for achieving a better catalytic activity.

Results of the BET measurements show that the specific surface area of the stoichiometric $LaFeO_3$ nanoperovskite does not change upon calcination at 900°C (Table 4). This characteristic of the nonstoichiometric samples, however, decreases more than 50% upon calcination at a higher temperature of 900°C. A decrease about one-third in the specific surface area of catalysts is observed with an increase in excess iron cations greater than 0.2 mole number. The excess iron cations are introduced as the main element of the agglomeration that causes a decrease in the specific surface area of samples. Among the calcined samples at 900°C, lanthanum ferrite with 0.2 mole excess iron cation and a specific surface area similar to the stoichiometric one decreases the light off temperature for CO oxidation about 70°C (samples 9 and 10 in Tables 3 and 4). The catalyst activity is slowly reduced on stream after abort 72 h. Activity of the catalyst after this time is about 90% of the fresh catalyst and a higher temperature is needed for the complete oxidation of carbon monoxide. The first activity is not reobtained after calcination of catalyst at 800°C. The perovskite structure, however, is not affecting over these reaction / temperature treatments. Thus, the activity decreasing can be related to the particle size increasing and area decreasing, which is under research.

Table 3. Catalytic performance, CO oxidation temperatures, for the prepared samples

	Temperature (°C) of CO Conversion		
Sample no.	10%	50%	90%
1	277	333	403
2	267	315	348
3	278	263	400
4	300	366	413
9	227	305	345
10	188	259	275
11	245	272	312
12	224	273	302

Table 5 shows the results of electrical conductivity measurements of samples 9-12. Electrical conductivity data were measured under isothermal steady state conditions at 400°C. A higher conductivity is observed for $LaFeO_3$ nanoperovskite under the oxidation atmosphere. Density of the charge carriers, however, decreases with an increase in the mole number of the excess iron cations, related to the crystalline phase of Fe_2O_3. Reducibility properties of samples 9-12 were studied using electrical conductivity measurements in oxidation (air) and reduction atmosphere (6%CO in Ar) at 400°C, respectively. Electrical conductivity measurements were carried out via switching the gas flow on the catalyst from air atmosphere to reduction atmosphere at 400°C. Data of σ_{Ox} and σ_{Red} were obtained under the steady

Table 4. BET, pore volume and pore diameter of samples of Table 1

Sample no.	1	2	3	4	9	10	11	12
BET (m^2/g)	14	27	20	23	14	14	8	8
Total pore volume (mL/g)	0.067	0.087	0.059	0.048	0.018	0.034	0.019	0.011
Average pore diameter (Å)	186	127	121	86	50	94	93	56

Table 5. Electric conductivity[a] results for the prepared samples after calcination at 900°C

Sample no.	σ_{ox}[b]×10^6 (Ω^{-1})	σ_{Red}[b]×10^6 (Ω^{-1})	σ_{Ox}/σ_{Red}	E_c (kCal/mol)
9	16.4	1.8	9.1	18.7
10	3.6	5.7	0.63	13.6
11	2.7	142.9	0.02	17.4
12	1.3	191.4	0.007	18.9

[a]Electric conductivity was measured at 300°C in which the conductivity under the oxidation atmosphere (σ_{ox}), i.e. air, was reached to a maximum.
[b]σ_{ox} and σ_{Red} are the conductivity under the oxidation (air) and reduction atmosphere (6%CO in Ar), respectively.

state conditions at 400°C (Table 5). A depletion of charge carriers has taken place during switching from air atmosphere to 6%CO in Ar atmosphere, decreasing the electrical conductivity of sample 9.

The charge carrier concentration, however, does not remarkably change for sample 10 and increases for samples 11-12 during switching from air to reducing atmosphere. The variation in the electrical conductivity behavior is related to the excess iron cations, dispersed in the form of Fe_2O_3 on the lanthanum ferrite. The mobile oxy anions can be considered as the main doer of the charge carriers in $LaFe_{(1+x)}O_{(3+\delta)}$ samples. Lanthanum ferrite is fully oxidized under oxidation atmosphere and the gained oxygen is not depleted suitably under reduction atmosphere. Crystalline Fe_2O_3, however, depletes the gained oxygen more readily than that of the lanthanum ferrite under reduction atmosphere. Small ration of σ_{Ox}/σ_{Red}, however, shows that the depleted oxy anions are not suitably replaced in samples with the excess iron cations greater than 0.2 mole number under oxidation atmosphere. Among the prepared samples, $LaFe_{1.2}O_{(3+\delta)}$ shows the best turnover in the giving and gaining oxy anions ($\sigma_{Ox}/\sigma_{Red} \sim 1$). An equilibrium condition for the exchange of oxy anions is reached for $LaFe_{1.2}O_{(3+\delta)}$ perovskite (sample 10) and is related to a better catalytic activity for CO oxidation (Tables 3 and 5).

An exponential increase in electrical conductivity of the samples with temperature is observed in air atmosphere [13]. Sample 10 with the best σ_{ox}/σ_{Red} and the lowest E_c is the most favorable one for reducibility and shows the best catalytic performance (see Tables 3 and 5). Here, E_c is defined as the activation energy of the electrical conductivity. It was obtained from a semi-Arrhenius plot ($Ln\sigma = -E_c/RT + Ln\sigma_0$) via the measurement of the electrical conductivity during the rise of temperature under air (oxidation) conditions. Results in Table 5 show that the conductivity of the lanthanum ferrite is affected by an increase in the mole number of the iron in the way we did in this study. An increase in the mole number of the iron cation in the $LaFeO_3$ sample up to 0.2 provides more suitable conditions for the oxygen transfer to the adsorbed CO on the catalyst surface.

CONCLUSION

Structural, magnetic and catalytic properties of $LaFe_{(1+x)}O_{(3+\delta)}$ (x = 0.0, 0.2, 0.5 and 0.7) nanoperovskites were investigated. Excess iron oxide is observed to be in the form of crystalline Fe_2O_3 phase. The $LaFe_{(1+x)}O_{(3+\delta)}$ catalysts can be considered as lanthanum ferrite with dispersed Fe_2O_3 over it. Temperature dependence of magnetization for $LaFe_{1.2}O_{(3+\delta)}$ shows a weak peak which is related to an insulator/insulator transition at the charge ordering temperature and is attributed to phase segregation. An increase in the iron content of $LaFeO_3$ perovskite up to 1.2 moles improves the electrical conductivity and oxidizing properties of the sample. Compared to the lanthanum ferrite, $LaFe_{1.2}O_{(3+\delta)}$ catalyst shows a higher performance in the oxidation of carbon monoxide. It relates to a better redox property that is observed for $LaFe_{1.2}O_{(3+\delta)}$ perovskite due to the charge ordering. The $LaFe_{1.2}O_{(3+\delta)}$ catalyst provides a better reaction pathway for electron and gas phase oxygen transfer from and to the adsorbed species on the catalyst surface.

ACKNOWLEDGMENTS

The authors are thankful to Frances Hellman, Laura Sposato, and Catherine Bordel for their help in magnetic measurements. This work was supported by the INSF (Grant No. 9004009) that is acknowledged.

CONFLICT OF INTEREST

The authors declare that there is no conflict of interests regarding the publication of this manuscript.

REFERENCES

[1] Y. Kumi, I. Kazuhiro, T. Akira, Medicine, 96(8), 6125 (2017).

[2] L. Gildo-Ortiz, J. Reyes-Gómez, J. M. Flores-Álvarez, H. Guillén-Bonilla, M. delaL.Olvera, V. M. Rodríguez Betancourtt, Y. Verde-Gómez, A. Guillén-Cervantes, J. Santoyo-Salazar, Ceram. Int., 42, 18821 (2016).

[3] P.L. Silveston, W.S. Epling, "Periodic Operation of Chemical Reactors", 2013, Chap. 6, "Automotive Exhaust Catalysis", 141.

[4] S. Gatla, D. Aubert, G. Agostini, O. Mathon, S. Pascarelli, T. Lunkenbein, M. G. Willinger, and H. Kaper, ACS Catal. 6 (9), 6151 (2016).

[5] Y. Maeda, T. Akita, M. Kohyama, Catal. Lett, 144 (12) 2086 (2014).

[6] M. F. M. Zwinkels, S. G. Järas, P. G. Menon, Catal. Rev. Sci. Eng. 35, 319 (1993).

[7] S. Vasala, M. Karppinen, Prog. Solid State Ch., 43, 1 (2015).

[8] C. Artini, J. Eur. Ceram. Soc., 37 (2), 427 (2017).

[9] R. Spinicci, A. Tofanari, A. Delmastro, D. Mazza, S. Ronchetti, Mater. Chem. Phys. 76, 20 (2002).

[10] S. M. Khetre, H. V. Jadhav and S. R. Bamane, Rasayan J. Chem., 3 (1), 82 (2010).

[11] D. Berger, C. Matei, G. Voicu, A. Bobaru, J. Eur. Ceram. Soc. 30, 617 (2010).

[12] E. Ghiasi, A. Malekzadeh, M. Ghiasi, J. Rare Eatrths, 31(10), 997 (2013).

[13] M. Khazaei, A. Malekzadeh, F. Amini, Y. Mortazavi, and A. Khodadadi, Cryst. Res. Technol. 45(10), 1064 (2010).

[14] L. Abadian, A. Malekzadeh, A. Khodadadi, Y. Mortazavi, Iran. J. Chem. Chem. Eng. 27, 71 (2008).

[15] [H. Bojari, A. Malekzadeh, M. Ghiasi, A. Gholizadeh, R. Azargohar, and A. K. Dalai, Cryst. Res. Technol. 48(6) 355 (2013)].

[16] W. Y. Zhao, P. Wei, H. B. Cheng, X. F. Tang, Q. J. Zhang, J. Am. Ceram. Soc., 90(7), 2095 (2007).

[17] G. Pecchi, C. Campos, O. Pena, Mater. Res. Bull. 44, 846 (2009).

[18] Z.X. Wei, Y.Q. Xu, H.Y. Liuc, C.W. Hu, J. Hazard. Mater. 165, 1056 (2009).

[19] M. Sivakumar, A. Gedanken, W. Zhong, Y.H. Jiang, Y.W. Du, I. Brukental, D. Bhattacharya, Y. Yeshurun, I. Nowik, J. Mater. Chem. 14, 764 (2004).

[20] J.Q. Li, Y. Matsui, S.K. Park, Y. Tokura, Phys. Rev. Lett. 79, 297 (1997).

[21] H.J. Xiang, M.H. Whangbo, Phys. Rev. Lett. 98, 246403 (2007).

[22] T. Misawa, J. Yoshitake, Y. Motome, Phys. Rev. Lett. 110, 246401 (2013).